

Journal of Biomedical Optics

BiomedicalOptics.SPIEDigitalLibrary.org

Monte Carlo investigation on quantifying the retinal pigment epithelium melanin concentration by photoacoustic ophthalmoscopy

Xiao Shu
Wenzhong Liu
Hao F. Zhang

Monte Carlo investigation on quantifying the retinal pigment epithelium melanin concentration by photoacoustic ophthalmoscopy

Xiao Shu,^a Wenzhong Liu,^a and Hao F. Zhang^{a,b,*}

^aNorthwestern University, Department of Biomedical Engineering, Evanston, Illinois 60208

^bNorthwestern University, Department of Ophthalmology, Chicago, Illinois 60611

Abstract. The retinal pigment epithelium (RPE) melanin plays an important role in maintaining normal visual functions. A decrease in the RPE melanin concentration with aging is believed to be associated with several blinding diseases, including age-related macular degeneration. Quantifying the RPE melanin noninvasively is therefore important in evaluating the retinal health and aging conditions. Photoacoustic ophthalmoscopy (PAOM), as an optical absorption-based imaging technology, can potentially be applied to measure variations in the RPE melanin if the relationship between the detected photoacoustic (PA) signal amplitudes and the RPE melanin concentrations can be established. In this work, we tested the feasibility of using PA signals from retinal blood vessels as references to measure RPE melanin variation using Monte Carlo (MC) simulation. The influences from PAOM axial resolution, the depth and diameter of the retinal blood vessel, and the RPE thickness were examined. We proposed a calibration scheme by relating detected PA signals to the RPE melanin concentrations, and we found that the scheme is robust to these tested parameters. This study suggests that PAOM has the capability of quantitatively measuring the RPE melanin *in vivo*. © 2015 Society of Photo-Optical Instrumentation Engineers (SPIE) [DOI: 10.1117/1.JBO.20.10.106005]

Keywords: retinal pigment epithelium; melanin; Monte Carlo simulation; photoacoustic imaging.

Paper 150405R received Jun. 15, 2015; accepted for publication Sep. 4, 2015; published online Oct. 15, 2015.

1 Introduction

Age-related macular degeneration (AMD) is a leading cause of irreversible vision loss among older adults in developed world.¹ Loss of the RPE melanin was reported to be associated with AMD.²⁻⁵ Melanin in the RPE absorbs most of the light passing through the pupil and helps scavenge free radicals,^{1,6} which protect macular region from oxidative stress.^{7,8} Therefore, developing an *in vivo* imaging method that can quantify the RPE melanin can be clinically significant.

In the past decades, researchers explored a number of methods to quantify RPE melanin.^{6,7,9-16} The spatial and temporal variations of RPE melanin concentration were successfully obtained by *in vitro* measurement. As the most direct approach, melanin concentration was roughly estimated by counting melanin granules from high-magnification micrograph⁹ or by counting the number of imaged pixels after Fontana-Masson staining.^{12,17} Later on, more accurate methods were developed. In electron spin resonance spectroscopy, spectrum of either ocular cell extracts or purified melanosomes was compared with the spectrum of synthetic DOPA melanin to determine the absolute melanin concentration.^{7,8} Optical absorption measurement was also reported to be employed after solubilization of free melanin granules *in vitro*.^{6,10,11} An indirect way to quantify melanin was to use high-performance liquid chromatography to measure the chemical reaction products of melanin and retrieve melanin concentration based on stoichiometric relationship.^{13,17} However, all

the above *in vitro* methods required invasive procedures on the RPE sample, which made them unsuitable for clinical application. In addition, the reported methods lacked consistency among themselves, possibly resulting from variations induced by inevitable extensive chemical or biological procedures. *In vitro* tissue fixation also changed the tissue properties, making melanin concentration measurement challenging.

To examine the RPE melanin concentration *in vivo*, fundus spectral analysis and near-infrared autofluorescence (NIR-AF) imaging were proposed.^{15,16,18} The spectrum of fundus optical reflectance was used to calculate melanin optical density based on an optical model of foveal reflection.¹⁶ However, its results were not consistent with physiological values due to oversimplified modeling of retinal tissue anatomy, optical scattering path lengths, and lack of depth resolution.¹⁹ The NIR-AF imaging has been suggested as an alternative to visualize ocular melanin because of the coincidence of strong AF signal and high melanin concentration in ocular tissues when excited by NIR light. However, a rigorous relationship between AF and melanin is still missing, and the AF signals from RPE and choroid are mixed due to the absence of depth resolution.¹⁸ A more reliable *in vivo* RPE melanin quantification method is still needed.

Photoacoustic imaging (PAI) is an emerging technology that can directly measure optical absorption properties in tissue.²⁰ The PA signal induced by illumination light is directly proportional to local optical energy deposition, which is related to tissue's optical absorption coefficient.²¹ The optical absorption coefficient, in turn, is linearly related to pigment concentration.^{6,22}

*Address all correspondence to: Hao F. Zhang, E-mail: hfzhang@northwestern.edu

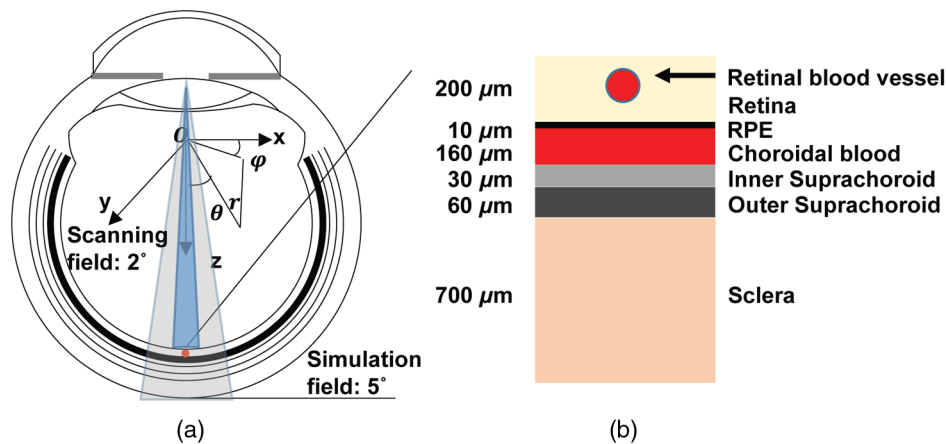


Fig. 1 Schematic of the eye model. (a) The geometry of the eye, optical illumination, recorded region of interest (ROI), and the coordinates. (b) Magnified view of the anatomical layers.

The ability of PAI to quantify endogenous chromophores has been investigated and confirmed by different research groups.^{23–25} Relative concentrations of both deoxy- and oxy-hemoglobin in blood vessels can be measured by PAI and be used to generate oxygen saturation map;^{23,25} PA method was also used to determine epidermal melanin content.²⁴

Photoacoustic ophthalmoscopy (PAOM) was recently developed for retinal imaging and was able to simultaneously visualize the structure and oxygen saturation of retinal blood vessels as well as RPE melanin distribution *in vivo*.^{21,26–28} Hence, PAOM has the potential to fill the technical void of quantifying RPE melanin *in vivo*. However, since external factors including variation of light source intensity, placement of transducer, and orientation of eye ball may affect the absolute detected PA signal,²¹ longitudinal monitoring of RPE melanin is challenging. A potential solution is to use PA signals from nearby blood vessels as a reference to the PA signals from the RPE. Because hemoglobin has well-defined optical absorption properties and patients' blood parameters, such as total hemoglobin concentration, are often easily accessible from routine blood examination, PA amplitudes from nearby vessels can be treated as an intrinsic reference to calibrate PA melanin measurements.

In this work, we applied Monte Carlo (MC) simulation of photon transport in the retina to test the feasibility of the aforementioned calibrated RPE melanin quantification using PAOM. First, we examined the optical energy deposition distribution across all retinal layers in an eye model. While it has long been suggested that the majority of light is absorbed by melanin in the RPE and choroid, yet no quantitative light absorption distribution model has been proposed. A finer retinal layers segmentation model was used, for the first time, to better mimic the ocular chromophores distribution.

Second, we examined the influence of PAOM axial resolution on the RPE melanin quantification. The RPE melanin together with choroidal melanin and choroidal blood are the main light absorbers in the posterior eye. Since melanin in the choroid does not vary much in life span and carries less known health value,⁶ only the RPE melanin is currently of clinical interest. However, the 2 layers are closely adjacent to each other and the RPE thickness is only around 10 μm .²⁹ The accuracy of measurement depends on the resolving power of PAOM along the axial direction, which is mainly determined by the ultrasonic transducer bandwidth.²⁰ We therefore investigated

the influence of PAOM axial resolution on the RPE melanin quantification.

Third, we examined the RPE melanin concentration calibration scheme. The detected absolute PA signal intensity depends on several parameters including local optical absorption, excitation laser intensity, and PA detection sensitivity. In order to accurately measure the local optical absorption, the variations of laser intensity and PA detection sensitivity should be compensated for. While laser intensity can be monitored in real time, PA detection sensitivity cannot be perfectly controlled across different experiments, since PAOM relies on optical scanning.²¹ For accurate *in vivo* melanin quantification, a calibration scheme must be developed. We proposed to use retinal blood measurement to calibrate melanin measurement and further determine RPE melanin concentration. Isobestic wavelengths for deoxy- and oxy-hemoglobin rule out the effects from variation of oxygen saturation level. Therefore, we selected the 570-nm and 584-nm as the excitation wavelengths.

Finally, we examined the influence of ocular parameters on the RPE melanin quantification. Multiple parameters, including the diameter and depth of the retinal blood vessel and the RPE layer thickness, may affect PAOM measurement. Based on our simulated results, we ruled out these concerns and validated the feasibility of our calibrated RPE melanin quantification scheme.

2 Methods and Materials

2.1 Eye Model

The posterior eye is often considered to consist of 4 anatomic layers: neural retinal layer, RPE, choroid, and sclera.^{30–32} In this study, our interest is the RPE, which is around 10 μm thick. In PAOM, optical absorption and scattering from neighboring layers, especially the highly optically absorbing choroid, will affect the detected PA signals from the RPE. Considering that choroid is not optically uniform, modeling choroid as a homogeneous layer will not provide the most accurate estimation of the RPE melanin in PAOM. We divided the choroid into 3 sublayers: one inner choroidal blood sublayer and 2 outer suprachoroid sublayers. Immediately below the Bruch membrane is the choroidal blood layer, which anatomically consists of choriocapillaris and 2 vascular layers (Haller's and Sattler's).³³ The inner choroid is thus optically modeled as homogeneous blood.³² Melanin is considered as the major

Table 1 Optical parameters used in Monte Carlo (MC) simulation.

| Wavelength (nm) | | Retina | RPE | ChB | ChMIn | ChMOut | Sclera | Vessel wall | Blood |
|-----------------|-----------------------------|--------|-------|-------|-------|--------|--------|-------------|-------|
| 570 | μ_a [mm ⁻¹] | 0.147 | 63 | 23.8 | 0.4 | 0.95 | 0.4 | 0.63 | 23.8 |
| | μ_s [mm ⁻¹] | 3.1 | 115.8 | 70 | 57.3 | 57.3 | 89.8 | 27.7 | 70 |
| | g | 0.97 | 0.84 | 0.972 | 0.87 | 0.87 | 0.9 | 0.86 | 0.972 |
| 584 | μ_a [mm ⁻¹] | 0.147 | 57.5 | 18.5 | 0.37 | 0.86 | 0.39 | 0.63 | 18.5 |
| | μ_s [mm ⁻¹] | 3.1 | 118.8 | 74.7 | 57.8 | 57.8 | 88.4 | 27.7 | 74.7 |
| | g | 0.97 | 0.84 | 0.972 | 0.87 | 0.87 | 0.9 | 0.86 | 0.972 |

optical absorber in suprachoroid, and the inner suprachoroid has lower melanin concentration than the outer suprachoroid.⁶

Figure 1 shows the eye model used in our MC simulation. The key parameters are as follows: eyeball diameter: 23.0 mm;³⁴ pupil illumination angle: 2 deg;³¹ retina thickness: 200 μm ; RPE thickness: 10 μm ;³⁰ choroidal blood layer thickness: 160 μm ; inner suprachoroid layer thickness: 30 μm ; outer suprachoroid layer thickness: 60 μm ;³³ and sclera layer thickness: 700 μm .³¹ We placed a cylindrical blood vessel segment (diameter: 100 μm) 10- μm beneath the retina surface,³⁰ and the vessel wall thickness was set to be 10% of the vessel lumen diameter.³⁵ Except for the finer division of the choroid layer, our eye model is similar to what used in previous studies.^{30-32,36} The wavelength-dependent optical absorption coefficients, scattering coefficients, and scattering anisotropy are extracted from the literatures^{6,11,31-33,36-40} and are summarized in Table 1. For the blood vessel, RPE, and the 3 choroid sublayers, we calculated the absorption coefficient based on hemoglobin (μ_a^H) and melanin concentration (μ_a^M) by

$$\mu_a^H = \ln(10) \times \text{Hb}_{\text{tot}} \times \left[\frac{\epsilon_{\text{HbO}_2} \times \text{sO}_2 + \epsilon_{\text{HbR}} \times (1 - \text{sO}_2)}{64,500} \right] \quad (1)$$

and

$$\mu_a^M = \ln(10) \times C_M \times \epsilon_M, \quad (2)$$

where Hb_{tot} (g/L) is the total hemoglobin concentration; sO_2 (dimensionless) is the oxygen saturation level; ϵ_{HbO_2} , ϵ_{HbR} , and ϵ_M (mm⁻¹/mol/L) are the molar extinction coefficients of oxy-hemoglobin, hemoglobin, and melanin, respectively; 64,500 (g/mol) is the molecular weight of hemoglobin; and C_M (mol/L) is the melanin concentration. In our simulation, we assumed that $\text{Hb}_{\text{tot}} = 150$ g/L,⁴¹ and set the sO_2 as 90% in blood of retinal vessel segment⁴² and 95% in choroidal blood.^{33,36}

As a simplified, yet, effective way of modeling, optical absorption within retinal blood and choroid blood layer is contributed only by hemoglobin (μ_a^H); optical absorption within the RPE and the 2 suprachoroidea layers are only from melanin (μ_a^M).³⁶ The wavelength-dependent extinction coefficients are obtained from published data.^{43,44} We neglected the refractive index difference in all the ocular layers.^{31,32} We simulated 570 and 584 nm illuminations, where absorption coefficients of the deoxy- and oxy-hemoglobin are the same. Thus, the absorption of the whole blood is independent of sO_2 , which

promises accurate reference signals for calibration in our imaging scheme.

2.2 Monte Carlo Simulation

In the MC simulation of photon transport, multiple photon packets are launched into tissue. Reflection or transmission takes place where there is a difference in the refractive indices. The optical scattering anisotropy and the total interaction coefficient determine the propagation direction and the path length between 2 consecutive photon-tissue interaction events,⁴⁵ while the ratio of absorption coefficient to the total interaction coefficient (albedo) determines the weight loss of photon packet at the location of interaction. At the location of each interaction event, the new photon packet propagation direction is calculated based on the local scattering anisotropy using the Henyey-Greenstein phase function. A photon packet is terminated when it travels outside the tissue or carries too little weight and does not survive the Russian Roulette rule.⁴⁵ Distribution of the energy deposition and diffuse reflectance of simulated region converge to the true value with increasing photon packets. The correctness of our homemade MC code was confirmed by comparing with previous published data using the same input.⁴⁵

In our PAOM simulation, photon packets were launched from the center of the pupil. The initial angle was randomly selected but will statistically follow a uniform distribution within the 2-deg field of view.^{30,31} Most previous studies considered the posterior eye flat when the illumination angle was sufficiently small. In our study, however, the curvature of the fundus was also considered and a spherical coordinate was used.³² As shown in Fig. 1(a), with the center of the eye ball being defined as the coordinate origin, our recorded region of interest (ROI) angle θ in the simulation was from 0 deg to 5 deg (2.5 times of the illumination angle); φ was from 0 deg to 360 deg; and r was from retina to sclera. To simulate PAOM, light energy deposition was recorded within the selected ROI.

2.3 Retinal Pigment Epithelium Melanin Concentration Measurement

PA signal amplitude is proportional to the product of Grüneisen coefficient Γ (the variation of Grüneisen coefficient in different retinal tissues is ignored), optical absorption coefficient μ_a , and the local optical fluence F .^{25,46} The ratio between PA amplitudes from the RPE (PA_{RPE}) and retinal blood vessel (PA_{Blood}) can be expressed as

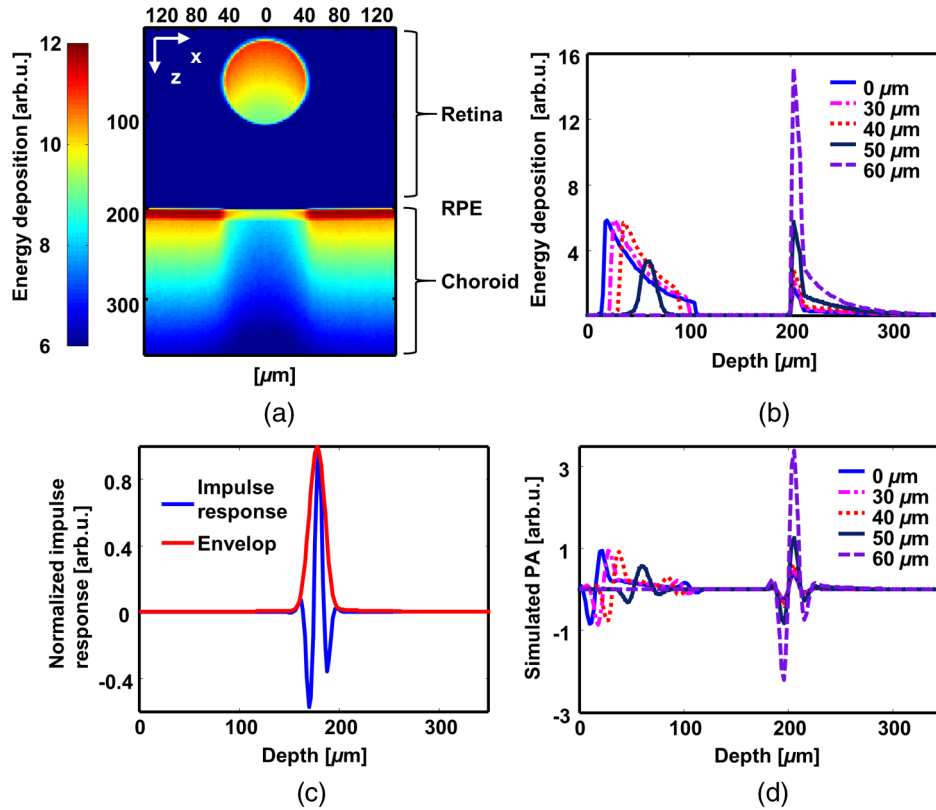


Fig. 2 Simulated optical absorption distribution and photoacoustic (PA) profile. (a) A representative B-scan image of energy deposition using 2.1 billion photon packets. The retinal pigment epithelium (RPE) melanin concentration is 300 mmol/L. (b) Representative A-lines of optical absorption at 5 different lateral positions with respect to the vessel center. (c) Simulated impulse response of a 75-MHz bandwidth ultrasonic detection system. (d) Simulated PA A-lines by convolving the energy deposition (b) with the impulse response (c).

$$\frac{PA_{RPE}}{PA_{Blood}} = \frac{\Gamma F_{RPE} \mu_a^{RPE}}{\Gamma F_{Blood} \mu_a^{Blood}}, \quad (3)$$

where PA_{Blood}/PA_{RPE} can be obtained from PAOM experiments; F_{RPE} and F_{Blood} are the optical fluences from an RPE region and a nearby vessel, which are similar, though not perfectly identical, given the small NA illumination in PAOM⁴⁷ and that retina is a thin tissue (200 μm) with weak optical scattering and absorption. In order to demonstrate the concept, we nevertheless get rid of the fluence terms and simplify Eq. (3) as

$$\mu_a^{RPE} = \mu_a^{Blood} \frac{PA_{RPE}}{PA_{Blood}}. \quad (4)$$

By combining Eqs. (2) and (4), the RPE melanin concentration can be estimated as

$$C_M^{RPE} = \mu_a^{Blood} \frac{PA_{RPE}}{PA_{Blood}} / \ln(10) \varepsilon_M, \quad (5)$$

where μ_a^{Blood} is the oxygen-saturation-dependent and can be calculated by Eq. (1). Both μ_a^{Blood} and ε_M are constant at a given optical wavelength. Therefore, the measured RPE melanin concentration is proportional to the PA amplitude ratio PA_{RPE}/PA_{Blood} , if neglecting fluence difference.

To verify the feasibility of RPE melanin quantification calibrated by retinal blood measurement in PAOM, we

numerically investigated the relationship between C_M^{RPE} and the PA amplitude ratio. We varied the RPE melanin concentration from 20 to 800 mmol/L, which covers all the reported concentrations.^{10,11}

2.4 Simulation of Energy Deposition and Photoacoustic Signal Ratio

We obtained the optical energy deposition distribution in the posterior eye and converted it into PA signal amplitude to simulate PAOM. During simulation, the posterior eye volume was discretized into voxels and optical energy deposition was scored into a 3-dimensional matrix, $A_{r\theta\varphi}[i_r, i_\theta, i_\varphi]$ (where r, θ, φ denote 3 dimensions in spherical coordinate, respectively). The voxel size was chosen to be 1 μm , much smaller than the actual system resolution. An arbitrary system axial resolution can be simulated by summing adjacent elements in r dimension of $A_{r\theta\varphi}$. The generated PA signal amplitude is proportional to energy deposition. Therefore, the PA amplitude ratio was obtained by taking the ratio of energy deposition at RPE and retinal blood vessel.

Admittedly, factors other than energy deposition also affect PA amplitude. However, by taking the ratio, we can rule out factors that influence PA amplitude at RPE and nearby vessel in a similar way, including, e.g., detection sensitivity and acoustic propagation loss. The effect of ultrasonic detection bandwidth was considered by defining system axial resolution. Though the shape and dimensions of optical absorber affect the generated PA amplitude, they were neglected in this

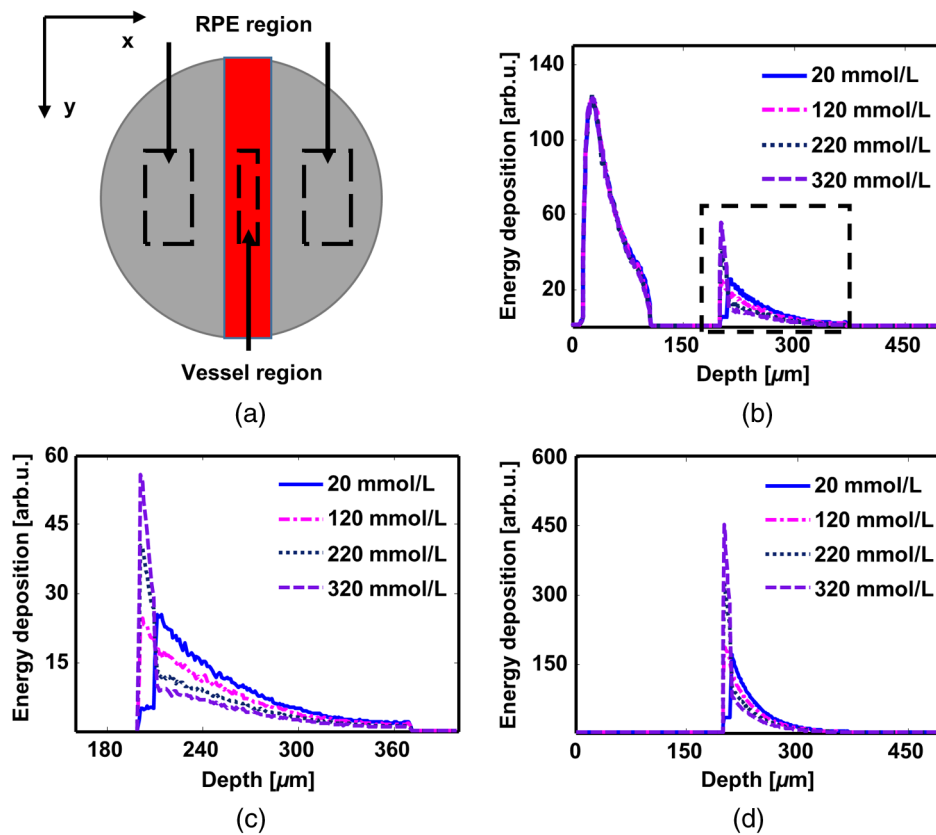


Fig. 3 Simulated depth-resolved profiles of energy deposition in VR and RR. Simulation results with different RPE melanin concentrations are shown in the same plot. (a) Vessel region (VR) and RR. It is a top-down view of simulation field. The red square is the retinal blood vessel while the gray background represents the RPE. (b) Depth-resolved profiles of energy deposition in VR. (c) A magnified view of the dashed square (b). (d) Depth-resolved profiles of energy deposition in RR.

simplified eye model, which contains only multiple homogeneous anatomical layers.

3 Results

3.1 Optical Energy Deposition Distribution

The simulated optical energy deposition in each anatomical layer is shown in Fig. 2. Figure 2(a) is a typical cross-sectional image of the distribution with the RPE melanin concentration at 300 mmol/L. Figure 2(b) shows the one-dimensional, depth-resolved optical absorption profiles extracted from Fig. 2(a) at different lateral positions with respect to the center of the blood vessel. Optical absorption in the retina mainly comes from the blood vessel. In regions outside the retinal blood vessel, the illuminating light does not encounter strong attenuation until reaching the RPE. Despite strong attenuation in the RPE, light can still penetrate into the inner choroid. Figure 2(c) shows a simulated impulse response of a 75-MHz bandwidth ultrasonic detection system. Figure 2(d) is the simulated PA A-lines of the energy deposition profiles in Fig. 2(b) obtained by convolving with impulse response.

To calculate the RPE melanin concentration, we divided the simulated field into the vessel region (VR) and the RPE region (RR) [Fig. 3(a)] within the x - y plane. Figure 3(b) shows the depth-resolved profiles of optical energy deposition in VR when we varied the RPE melanin concentration from 20 to 320 mmol/L. The RPE absorption increases with the increment

of RPE melanin concentration, while the choroid absorption decreases. Figure 3(c) is the magnified view of the dashed box. Figure 3(d) shows the depth-resolved profiles of optical energy deposition in RR, where the absorption in retina is negligible. The shapes of the lines are analogous to that in Fig. 3(c).

We investigated the influence of the RPE melanin concentration on relative optical energy deposition in different posterior eye layers. Figure 4(a) shows the axial energy deposition distribution in VR, and Fig. 4(b) shows the distribution in RR. In VR, the vessel absorbs around 80% of total incident light energy. In RR, inner choroid absorbs the majority of the light until melanin concentration in RPE increases to around 300 mmol/L. Light is not able to penetrate through choroidal blood and reach outer choroid even if RPE melanin concentration is really low.

3.2 Influence of Photoacoustic Ophthalmoscopy Axial Resolution

Mathematically, an ideal linear dependence of the measured RPE melanin concentration on detected PA signal amplitude ratio (Sec. 2) is valid only when PAOM has infinite axial resolution. In practice, such linear dependence can vary considering the finite size of PAOM axial resolution. To investigate the influence of axial resolution, we integrated simulated energy deposition over a depth range corresponding to a practical axial resolution and tested the relationship between RPE melanin concentration and PA signal amplitude ratio.

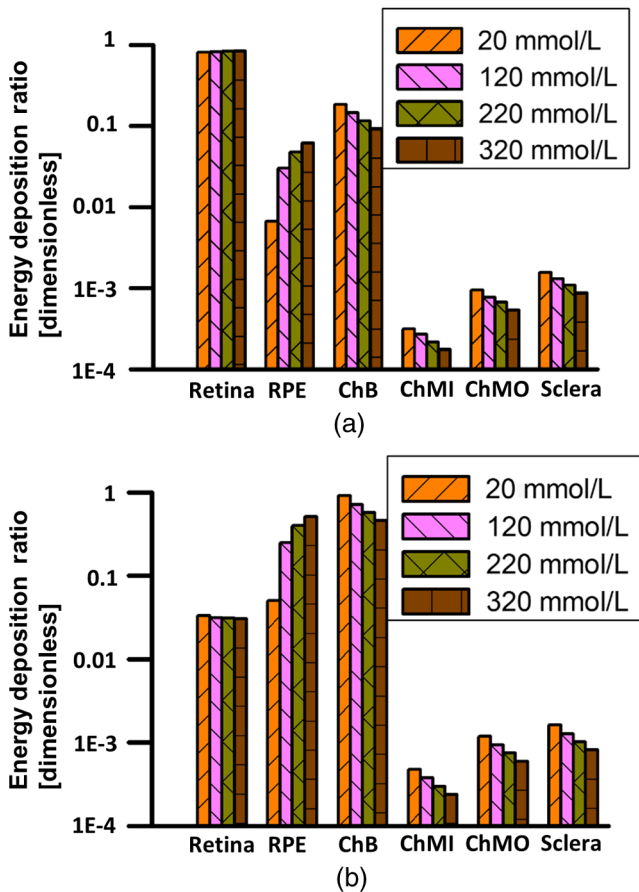


Fig. 4 Relative optical energy deposition in posterior eye layers with varied RPE melanin concentration. ChB, ChMI, and ChMO stand for choroidal blood layer, inner suprachoroid and outer suprachoroid, respectively. (a) Relative energy deposition in VR. (b) Relative energy deposition in RR. The vertical axes are plotted in logarithmic scale.

We varied the axial resolution from 10 μm to 30 μm . When PAOM cannot resolve the 10- μm thick RPE layer, the detected PA signal contains contributions from both the RPE and choroid. Figure 5(a) shows the ratio of RPE-generated PA signal to total signal generated within axial resolution. It indicates

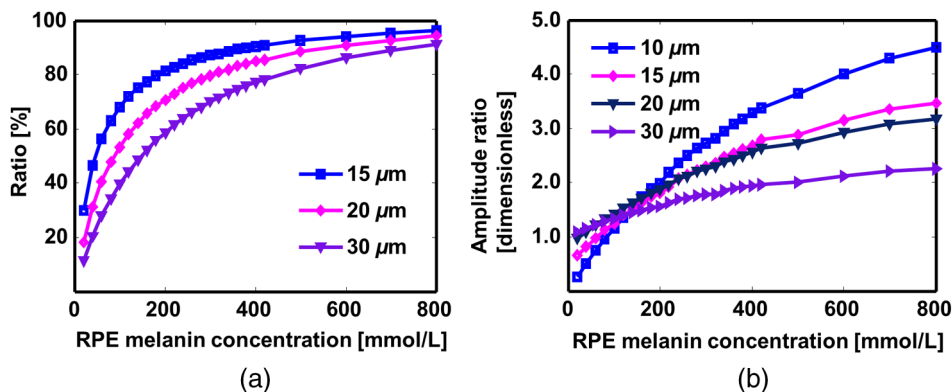


Fig. 5 The influence of photoacoustic ophthalmoscopy (PAOM) axial resolution on the PA signal amplitude ratio. The simulated RPE thickness is 10 μm . (a) Percentage of RPE contribution to PA signal generated at RPE-choroid. (b) Calibration curves of amplitude ratio with different RPE melanin concentrations. PAOM cannot resolve RPE layer until axial resolution is as small as 10 μm . 570-nm excitation wavelength is used.

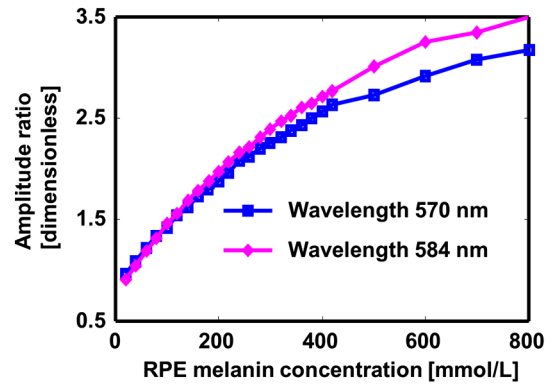


Fig. 6 The influence of illumination wavelength. The axial resolution of PAOM is 20 μm .

that when the RPE melanin concentration is low, the detected signal comes more from the choroid than RPE.

We varied the RPE melanin concentrations and investigated its effect on PA signal amplitude ratio, as shown in Fig. 5(b). Note that PA_{RPE} always involves possible contribution from choroidal blood. The RPE thickness is 10 μm ; therefore, the PA signal is purely from RPE when the axial resolution is 10 μm . The ratio increases with RPE melanin concentration. But when the axial resolution is worse than 10 μm , the ratio becomes less sensitive to the change in RPE melanin. This is because absorption from choroidal blood is involved.

3.3 Influence of Excitation Wavelength

Isosbestic wavelengths for oxy-hemoglobin and hemoglobin are better suited for measurement since the blood absorption can be independent of oxygen saturation level. There are multiple wavelengths that satisfy this requirement,⁴³ among them 570 and 584 nm are the best choices because of relatively strong optical absorption. Figure 6 shows the amplitude ratio curves for 570 and 584 nm with the preset 20- μm axial resolution. There is no significant difference between the 2 wavelengths, especially when the RPE melanin concentration is not extremely high.

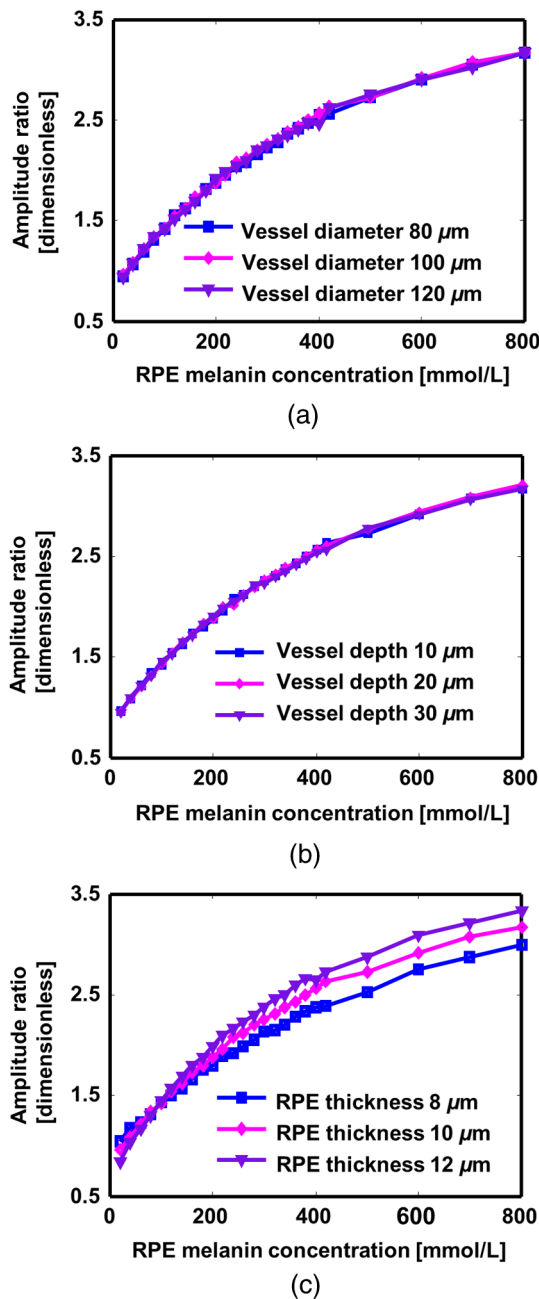


Fig. 7 The influence of retinal parameters variations on PA signal amplitude ratio. (a) Influence of the retinal blood vessel diameter. (b) Influence of the retinal blood vessel depth with regard to retina surface. (c) Influence of the RPE thickness.

3.4 Influence of Anatomical Variations

Anatomical variations in eye are reported among individuals,^{29,30,34} which may affect measurement. To test the robustness of the RPE melanin quantification by PAOM, we varied the depth and diameter of the retinal blood vessel as well as the RPE thickness in the eye model. The axial resolution was set at 20 μm.

Figure 7(a) shows the relationship between the amplitude ratio curves with varied retinal blood vessel size. Three curves are roughly identical despite $\pm 20\%$ variation of vessel diameter. Figure 7(b) shows that the depth of the blood vessel in retina

barely affects the ratio curve. This is because of weak absorbing and scattering from retina tissue.

Figure 7(c) shows that the RPE thickness would influence the ratio curve. Since the 20-μm axial resolution of PAOM is not able to resolve RPE layer, the detected PA signal is an integration of energy deposition in RPE and inner choroid. When the RPE melanin concentration is high, the absorption coefficient of RPE is larger than that of inner choroid, a thicker RPE will generate stronger PA signal and lead to a larger amplitude ratio. Otherwise, when RPE melanin concentration is low, the absorption coefficient of choroid is larger; a thicker RPE leads to a weaker PA signal and a smaller amplitude ratio. The 3 curves cross at the same point, where absorption coefficients of 2 layers are the same and the amplitude ratio is almost independent of RPE thickness.

4 Discussion

4.1 Retinal Pigment Epithelium Melanin Concentration

The simulation provides a moderate reference for possible *in vivo* RPE melanin concentration. So far, no consistency on the absolute RPE melanin concentration can be found from the literature. In the previous MC ocular simulations, difference in the assumed RPE melanin concentration can be as large as 3 orders of magnitude. Preece and Claridge assumed that the RPE melanin concentration is around 5 mmol/L,³⁶ whereas in the work of Guo et al., simulation was conducted with the RPE melanin concentration from 0.8 to 4 mol/L.³² Experimental studies by Schmidt and Peisch showed that for normal human, melanin concentration is around 200 mmol/L in macular region and higher concentration is expected in peripheral regions.¹¹ In a more recent study, Durairaj et al. reported 60 to 100 mmol/L melanin in human choroid-RPE.¹⁰ Both of their measurements were *in vitro*, yet enucleation of eye and solubilization of melanin were performed before measurements, where the accuracy of results might be affected. In our work, we varied RPE melanin concentration from 20 to 800 mmol/L, which covered the range of reported data and very likely, physiological condition.

The study confirms that the strong optical absorption by the RPE is the foundation of melanin quantification using PAOM. Total light absorption in the RPE is less than choroidal vasculatures unless the RPE melanin concentration reaches around 300 mmol/L. But the deposited energy density in the RPE is usually higher. This, indeed, allows PAOM to quantify the RPE melanin even though the axial resolution cannot resolve the boundary between the RPE and choroid.

4.2 Retinal Pigment Epithelium Melanin Measurement with Photoacoustic Ophthalmoscopy

Our proposal is to determine the absolute RPE melanin concentration through the ratio of PA signal amplitudes between the RPE and a nearby blood vessel. As indicated in previous section, this ratio should be linearly related to the RPE melanin concentration, assuming the same optical fluence for retinal blood vessel and RPE, and infinite system resolution. However, in reality, the same fluence assumption only holds true for infinitely thin layers on the top boundary of blood vessels and the uppermost

surface of the RPE. For tissue volume deeper than the superficial layers, optical fluences are subjected to a roughly exponential decay governed by Beer's law. Such decays are not negligible due to strong optical absorption in retinal blood vessel and the RPE. The PA detected signal is a result of integrating energy deposition within a resolution-determined tissue volume. Though the initial optical fluence in blood vessel and the RPE is the same, different decay rates lead to different energy depositions within integration volume.⁴⁸ Therefore, for any finite system resolution, the linear dependence of amplitudes ratio on RPE melanin concentration can still be affected. In addition, the axial resolution of PAOM is typically 23 μm ,²¹ which is not capable of resolving such a thin layer as RPE. This leads to the fact that the detected PA signals from the RPE are a combination of signals from the RPE and the choroid beneath. Both of these effects degrade the linear relationship.

Despite influence from uneven optical fluence and finite PAOM axial resolution, the ratio is uniquely determined theoretically and can serve as a good practical measure of the RPE melanin concentration. The range of ratio we got from the simulation agrees with previous published experimental data.²⁷ Though the data are obtained from rats, Durairaj et al.¹⁰ show that difference in RPE melanin concentration across different species exists, but generally on the same order of magnitude.

Desired wavelengths of PAOM measurement are proposed. Wavelengths of 570 and 584 nm are ideal for PA excitation because the absorption coefficient of blood is independent of SO_2 . The differences between the amplitude ratio curves for 2 wavelengths are 2.1% when the RPE melanin concentration is below 200 mmol/L, 5.8% when the RPE melanin concentration is between 200 and 400 mmol/L, and 9.5% when the RPE melanin concentration is between 400 and 800 mmol/L.

Simulation suggests that the proposed method is robust to variations in retinal blood vessels. 20% change in vessel diameter only results in less than 0.4% difference in curves of amplitude ratio. The variation of RPE thickness will affect the curve significantly, especially when melanin concentration is high. Study shows that RPE thickness is in a narrow range among population, $11 \pm 2 \mu\text{m}$,²⁹ which is covered by simulation. The RPE thickness can be measured by optical coherence tomography (OCT), which achieves as high depth resolution as 1 μm .⁴⁹

Quantification of the RPE melanin concentration by PAOM has several benefits. First, the capability of *in vivo* measurement makes it suitable for clinical diagnosis. Second, the signal detected in PAOM is directly related to the tissue absorption coefficient, and thus melanin concentration and no complicated modeling are involved. Finally, PAOM, whether integrated with other imaging modalities or not, can provide diagnosis information from multiple aspects.

4.3 Ocular Light Absorption Distribution and Retinal Pigment Epithelium Melanin Concentration

Besides the quantification method, this study helps to establish a thorough understanding, from light-absorption point of view, of the tissue-photon interaction at posterior segment of human eye, which may provide insight to different roles played by hemoglobin, the RPE, and choroid melanin. The large retinal blood vessels absorb the majority of photons at the surface of retina, whereas choriocapillaris and vascular layers absorb all the light that transmits through the RPE. Compared with the RPE melanin, which is a major photon absorber, the

choroidal melanin mostly concentrated in the outer choroid, absorbs barely any light. Lack of interaction with light might explain the constant choroidal melanin content during the life span.⁶

5 Conclusion

We conducted MC simulation to investigate light propagation and energy deposition in posterior eye, and tested the feasibility of using PAOM to quantify the RPE melanin concentration. The simulation was based on an improved eye model with finer anatomical separation in the choroid. We investigated the change of PA signal amplitude ratio between the RPE and the retinal blood vessel with varied RPE melanin concentrations. The current investigation can provide insights in future experimental research. Though not required, an axial resolution that could resolve the RPE layer is desired for measurement with higher sensitivity. It is better to integrate PAOM with other imaging modality, especially high-resolution OCT to compensate for variation of RPE thickness.

Acknowledgments

The authors thank Siyu Chen, Dr. Ji Yi, Dr. Biqin Dong, and Christina Chan for insightful comments. The authors would like to acknowledge the generous financial support from NIH under Grant Nos. 1R01EY019951, 1R24EY022883, and 2R01EY019484; and NSF under Grant Nos. CBET-1055379 and DBI-1353952. Wenzhong Liu is supported by the Howard Hughes Medical Institute International Research Fellowship. We also acknowledge the computational resources and staff contributions provided by the Quest High-Performance Computing Facility at Northwestern University. Hao F. Zhang has financial interests in Opticent Health Inc., which, however, did not support this work.

References

1. N. M. Bressler, S. B. Bressler, and S. L. Fine, "Age-related macular degeneration," *Survey Ophthalmol.* **32**(6), 375–413 (1988).
2. T. T. Berendschot et al., "Influence of lutein supplementation on macular pigment, assessed with two objective techniques," *Invest. Ophthalmol. Visual Sci.* **41**(11), 3322–3326 (2000).
3. R. A. Bone et al., "Lutein and zeaxanthin in the eyes, serum and diet of human subjects," *Exp. Eye Res.* **71**(3), 239–245 (2000).
4. J. T. Landrum, R. Bone, and M. D. Kilburn, "The macular pigment: a possible role in protection from age-related macular degeneration," *Adv. Pharmacol.* **38**, 537–556 (1996).
5. L. G. Hyman et al., "Senile macular degeneration: a case-control study," *Am. J. Epidemiol.* **118**(2), 213–227 (1983).
6. J. Weiter et al., "Retinal pigment epithelial lipofuscin and melanin and choroidal melanin in human eyes," *Invest. Ophthalmol. Visual Sci.* **27**(2), 145–152 (1986).
7. T. Sarna et al., "Loss of melanin from human RPE with aging: possible role of melanin photooxidation," *Exp. Eye Res.* **76**(1), 89–98 (2003).
8. A. Zadto et al., "Photobleaching of retinal pigment epithelium melanosomes reduces their ability to inhibit iron-induced peroxidation of lipids," *Pigment Cell Res.* **20**(1), 52–60 (2007).
9. L. Feeney-Burns, E. Hilderbrand, and S. Eldridge, "Aging human RPE: morphometric analysis of macular, equatorial, and peripheral cells," *Invest. Ophthalmol. Visual Sci.* **25**(2), 195–200 (1984).
10. C. Durairaj, J. E. Chastain, and U. B. Kompella, "Intraocular distribution of melanin in human, monkey, rabbit, minipig and dog eyes," *Exp. Eye Res.* **98**, 23–27 (2012).
11. S. Y. Schmidt and R. D. Peisch, "Melanin concentration in normal human retinal pigment epithelium. Regional variation and age-related reduction," *Invest. Ophthalmol. Visual Sci.* **27**(7), 1063–1067 (1986).

12. W. Kang et al., "Melasma: histopathological characteristics in 56 Korean patients," *Br. J. Dermatol.* **146**(2), 228–237 (2002).
13. S. Ito and K. Jimbow, "Quantitative analysis of eumelanin and pheomelanin in hair and melanomas," *J. Invest. Dermatol.* **80**(4), 268–272 (1983).
14. J. R. Sparrow et al., "Quantitative fundus autofluorescence in mice: correlation with HPLC quantitation of RPE lipofuscin and measurement of retina outer nuclear layer thickness," *Invest. Ophthalmol. Visual Sci.* **54**(4), 2812–2820 (2013).
15. M. J. Kanis, T. T. Berendschot, and D. van Norren, "Influence of macular pigment and melanin on incident early AMD in a white population," *Graefe's Arch. Clin. Exp. Ophthalmol.* **245**(6), 767–773 (2007).
16. T. T. Berendschot et al., "Macular pigment and melanin in age-related maculopathy in a general population," *Invest. Ophthalmol. Visual Sci.* **43**(6), 1928–1932 (2002).
17. T. Tadokoro et al., "UV-induced DNA damage and melanin content in human skin differing in racial/ethnic origin," *FASEB J.* **17**(9), 1177–1179 (2003).
18. C. N. Keilhauer and F. C. Delori, "Near-infrared autofluorescence imaging of the fundus: visualization of ocular melanin," *Invest. Ophthalmol. Visual Sci.* **47**(8), 3556–3564 (2006).
19. J. van de Kraats, T. T. Berendschot, and D. van Norren, "The pathways of light measured in fundus reflectometry," *Vision Res.* **36**(15), 2229–2247 (1996).
20. H. F. Zhang et al., "Functional photoacoustic microscopy for high-resolution and noninvasive in vivo imaging," *Nat. Biotechnol.* **24**(7), 848–851 (2006).
21. H. F. Zhang, C. A. Puliafito, and S. Jiao, "Photoacoustic ophthalmoscopy for in vivo retinal imaging: current status and prospects," *Ophthalmic Surg. Lasers Imaging* **42**, S106–S115 (2011).
22. R. R. Anderson and J. A. Parrish, "The optics of human skin," *J. Invest. Dermatol.* **77**(1), 13–19 (1981).
23. L. V. Wang and S. Hu, "Photoacoustic tomography: in vivo imaging from organelles to organs," *Science* **335**(6075), 1458–1462 (2012).
24. J. A. Viator et al., "A comparative study of photoacoustic and reflectance methods for determination of epidermal melanin content," *J. Invest. Dermatol.* **122**(6), 1432–1439 (2004).
25. Z. Guo, S. Hu, and L. V. Wang, "Calibration-free absolute quantification of optical absorption coefficients using acoustic spectra in 3D photoacoustic microscopy of biological tissue," *Opt. Lett.* **35**(12), 2067–2069 (2010).
26. W. Song et al., "In vivo photoacoustic chorioretinal vascular imaging in albino mouse," *Chin. Opt. Lett.* **12**(5), 051704 (2014).
27. X. Zhang et al., "Simultaneous in vivo imaging of melanin and lipofuscin in the retina with photoacoustic ophthalmoscopy and autofluorescence imaging," *J. Biomed. Opt.* **16**(8), 080504 (2011).
28. W. Song et al., "A combined method to quantify the retinal metabolic rate of oxygen using photoacoustic ophthalmoscopy and optical coherence tomography," *Sci. Rep.* **4**, (2014).
29. C. W. Spraul, G. E. Lang, and H. E. Grossniklaus, "Morphometric analysis of the choroid, Bruch's membrane, and retinal pigment epithelium in eyes with age-related macular degeneration," *Invest. Ophthalmol. Visual Sci.* **37**(13), 2724–2735 (1996).
30. W. Liu, S. Jiao, and H. F. Zhang, "Accuracy of retinal oximetry: a Monte Carlo investigation," *J. Biomed. Opt.* **18**(6), 066003 (2013).
31. M. Hammer et al., "Light paths in retinal vessel oximetry," *IEEE Trans. Biomed. Eng.* **48**(5), 592–598 (2001).
32. Y. Guo et al., "Monte Carlo model for studying the effects of melanin concentrations on retina light absorption," *J. Opt. Soc. Am. A* **25**(2), 304–311 (2008).
33. D. L. Nickla and J. Wallman, "The multifunctional choroid," *Progr. Retinal Eye Res.* **29**(2), 144–168 (2010).
34. C. R. Nave, *HyperPhysics*, <http://hyperphysics.phy-astr.gsu.edu/hbase/vision/eyescal.html> (3 February 2013).
35. M. Ritt and R. E. Schmieder, "Wall-to-lumen ratio of retinal arterioles as a tool to assess vascular changes," *Hypertension* **54**(2), 384–387 (2009).
36. S. J. Preece and E. Claridge, "Monte Carlo modelling of the spectral reflectance of the human eye," *Phys. Med. Biol.* **47**(16), 2863 (2002).
37. N. Bosschaart et al., "A literature review and novel theoretical approach on the optical properties of whole blood," *Lasers Med. Sci.* **29**(2), 453–479 (2014).
38. M. Hammer, A. N. Yaroslavsky, and D. Schweitzer, "A scattering phase function for blood with physiological haematocrit," *Phys. Med. Biol.* **46**(3), N65 (2001).
39. M. Keijzer et al., "Fluorescence spectroscopy of turbid media: autofluorescence of the human aorta," *Appl. Opt.* **28**(20), 4286–4292 (1989).
40. M. Hammer et al., "Optical properties of ocular fundus tissues—an in vitro study using the double-integrating-sphere technique and inverse Monte Carlo simulation," *Phys. Med. Biol.* **40**(6), 963 (1995).
41. J. D. Cook et al., "Estimates of iron sufficiency in the US population," *Blood* **68**(3), 726–731 (1986).
42. S. H. Hardarson et al., "Oxygen saturation in human retinal vessels is higher in dark than in light," *Invest. Ophthalmol. Visual Sci.* **50**(5), 2308–2311 (2009).
43. S. Prahl, "Optical absorption of hemoglobin," *Oregon Medical Laser Center*, <http://omlc.org/spectra/hemoglobin/> (3 February 2013).
44. S. Jacques, "Extinction coefficient of melanin," <http://omlc.org/spectra/melanin/extcoeff.html> (3 February 2013).
45. L. Wang, S. L. Jacques, and L. Zheng, "MCML—Monte Carlo modeling of light transport in multi-layered tissues," *Comp. Methods Progr. Biomed.* **47**(2), 131–146 (1995).
46. J. Yao and L. V. Wang, "Sensitivity of photoacoustic microscopy," *Photoacoustics* **2**(2), 87–101 (2014).
47. S. Jiao et al., "Photoacoustic ophthalmoscopy for in vivo retinal imaging," *Opt. Express* **18**(4), 3967–3972 (2010).
48. J. Wang et al., "Saturation effect in functional photoacoustic imaging," *J. Biomed. Opt.* **15**(2), 021317 (2010).
49. W. Drexler et al., "Ultrahigh-resolution ophthalmic optical coherence tomography," *Nat. Med.* **7**(4), 502–507 (2001).

Biographies of all the authors are not available.